Qualitative analysis of the dynamics of the time delayed Chua's circuit

Qualitative Analysis of the Dynamics of the Time-Delayed Chua's Circuit

Mario Biey, Fabrizio Bonani, *Member, IEEE*, Marco Gilli, *Member, IEEE*, and Ivan Maio

***Abstract*— Several variants of the Chua's circuit have been recently proposed in order to enlarge the class of nonlinear phenomena that can be generated by relatively simple circuits. In particular, Sharkovsky *et al.* proposed the so called time-delayed Chua's circuit (TDCC), where the original lumped LC resonator is substituted by an ideal transmission line, thereby generating an infinite dimensional system. The TDCC has been studied in details in the absence of the capacitor C, the only lumped dynamic element left in the circuit. This paper studies the effects of the presence of C on the dynamics of the circuit. After recasting the circuit equations in a suitable normalized form, their characteristic equation is theoretically investigated and the regions in the parameter space where all the eigenvalues have negative real part are exactly evaluated along with all the possible qualitative eigenvalue distributions. This analysis allows for a qualitative description of the TDCC dynamics in presence of the capacitor C. In particular, it is shown that, for particular sets of circuit parameters, an even *small* value of C, e.g., a parasitic element, may completely change the behavior of TDCC and that, on the other hand, any TDCC, exhibiting the period-adding phenomenon for $C = 0$, still continues to present this phenomenon even if a *small* capacitor C is added to the circuit.**

***Index Terms*—Bifurcation, chaos, nonlinear circuits.**

I. Introduction

IN THE LAST few years, a great deal of interest has been focused on exploring the complex dynamics of nonlinear circuits.

Chua's circuit has been widely studied in this context, for its capability to show a great variety of behaviors observable in other more complicated nonlinear circuits and as the structurally simplest autonomous electric circuit which may produce chaotic signals. Recently, variants of this circuit have been investigated, to enlarge the class of nonlinear phenomena that can be generated by relatively simple circuits [1]–[8].

In particular, the work of Sharkovsky *et al.* [1], [2] increases the dimension of the state space by substituting the lumped LC resonator with an ideal (i.e., lossless) transmission line (TL); furthermore, a dc voltage source is series connected to the piecewise linear resistor (Fig. 1) in order to break the symmetry in the original Chua's diode v–i characteristic.

This circuit, hereafter called the time-delayed Chua's circuit (TDCC), has been studied in details for $C = 0$ [1], [2], [8].

Manuscript received January 22, 1996; revised August 27, 1996. This work was supported in part by Ministero dell'Università e della Ricerca Scientifica under the National Research Plan 40% of the year 1994, and by Consiglio Nazionale delle Ricerche, Rome, Italy, under contribution 9 400 015.CT07. This paper was recommended by Associate Editor O. Feely.

The authors are with the Dipartimento di Elettronica, Politecnico di Torino, Torino, I-10129 Italy.

Publisher Item Identifier S 1057-7122(97)04403-6.

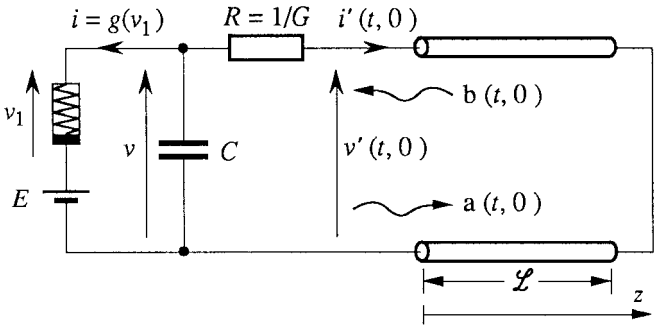

Fig. 1. TDCC.

In this case, the equations may be reduced to one nonlinear difference equation with a continuous argument and the circuit exhibits chaotic behaviors similar to those observable in "dry" systems, i.e., in absence of viscosity [9].

The presence of C leads to a nonlinear *differential*-difference equation [1], [10], which does not admit a complete analytical treatment (see [11]). So far, some partial results on the qualitative behavior of the circuit have been reported in [10] and [12].

The purpose of this paper is to explore the behavior of TDCC as the capacitance is varied, supporting extensive numerical simulations by a theoretical analysis of the circuit characteristic equation. In Section II, the circuit equations are recasted in a suitable form, valid for both $C = 0$ and $C \neq 0$. In Section III, the case $C = 0$ is briefly summarized, and the link between the circuit dynamics and the component values is reviewed through a detailed discussion of the related 1-D maps. Finally, in Section IV, the effects of the capacitor are examined by studying the circuit characteristic equation in each region of linearity, which allows for a qualitative analysis of TDCC dynamics.

II. Circuit Equations

The TDCC and the Chua's diode characteristic are shown in Figs. 1 and 2, respectively, where the variables involved in the analysis are also defined. A constant voltage generator E is inserted in series with the Chua's diode, to shift its original v–i characteristic along the axis of the capacitor voltage v. The parameters of the circuit are the round trip delay T and the characteristic impedance Z of the TL, the slopes m_0, m_1, m_{-1}, and the switching voltage B_p of the Chua's diode, the source voltage E, and the lumped linear elements C and G. The line parameters relate to the line per-unit-length inductance ℓ and

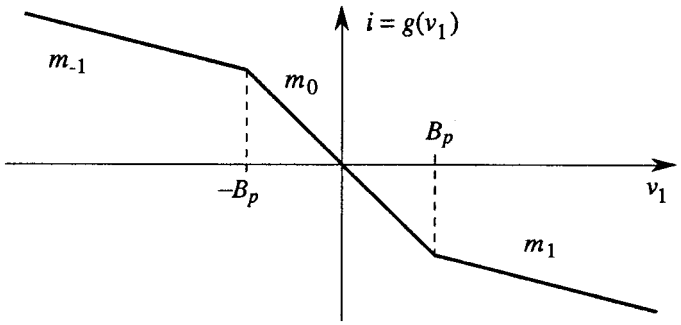

Fig. 2. Piecewise linear characteristic of the Chua's diode.

capacitance c, and to the line length $\mathcal{L}$ as $T = 2\mathcal{L}\sqrt{\ell c}$ and $Z = \sqrt{\ell/c}$.

The equations describing the lumped part of the network are

$$C\frac{\mathrm{d}v}{\mathrm{d}t} + g(v(t) - E) + i'(t,0) = 0$$
$$G[v(t) - v'(t,0)] = i'(t,0) \tag{1}$$

where $g(\cdot)$ is the piecewise-linear function represented in Fig. 2. As a consequence, the TDCC is a piecewise-linear circuit with three regions of linear operation, selected by the value of $v_1 = v - E$. For $v_1 < -B_p, |v_1| \leq B_p$ and $v_1 > B_p$, the Chua's diode operates on its leftmost, central and rightmost linear branch, respectively. In the following, these regions of linear operation are indicated by $\mathcal{R}_{-1}, \mathcal{R}_0$ and $\mathcal{R}_1$, respectively. In the linear region $\mathcal{R}_q$ the function $g(v_1)$ of Fig. 2 is expressed by $g(v_1) = m_q v_1 + \Delta m_q$, where $\Delta m_q = q(m_0 - m_q)B_p$, and $q = -1, 0, 1$. For the sake of simplicity, in this paper we assume $m_{-1} = m_1$ and $B_p = 1$, so that $\Delta m_q = q(m_0 - m_q)$.

Resorting to the voltage waves $a(t,z)$ and $b(t,z)$ associated to $v'(t,z)$ and $i'(t,z)$:

$$v'(t,z) = a(t,z) + b(t,z)$$
$$i'(t,z) = [a(t,z) - b(t,z)]/Z \tag{2}$$

the input characteristic of the TL is effectively expressed by the constraint

$$b(t,0) = -a(t - T, 0). \tag{3}$$

Since the line variables are considered only at $z = 0$, the z argument will be dropped hereafter.

The first set of circuit equations is obtained by replacing v' and i' of (1) with their voltage wave expressions (2), subject to constraint (3):

$$C\frac{\mathrm{d}v}{\mathrm{d}t} + g(v(t) - E) + \frac{v(t)}{R+Z} = \frac{2}{R+Z}b(t) \tag{4}$$

$$a(t) = \frac{R-Z}{R+Z}b(t) + \frac{Z}{R+Z}v(t) \tag{5}$$

$$b(t+T) = -a(t) \tag{6}$$

where $R = 1/G$.

This set of equations has some convenient features. First, the inclusion of the lumped capacitor affects only (4), through the presence of the differential term. Second, the equations allow a scattering interpretation of the problem and can be effectively exploited in the numerical simulation of the circuit response.

A simple description of the scattering process starts from (5), which yields the signal $a(t)$ injected into the TL as a sum of a contribution from the reflection of the signal $b(t)$, coming out of the line, and a contribution from the transmission of the signal $v(t)$. Voltage $v(t)$, in turn, is determined by $b(t)$ up to time t through (4). The last equation (6), here kept separate from (5) to highlight its physical meaning, is the reflection equation of the distortionless line.

The numerical solution of the equations is obtained through a recursive procedure suggested by the scattering process. The time axis is divided into left open time intervals $I_n =](n-1)T, nT]$, lasting one line delay T. Starting from the initial condition $v(0), b(t)$ assigned for $t \in I_1$ (that is the signal outcoming from the TL in $]0,T]$), (4) is solved obtaining $v(t)$ in I_1, then $b(t)$ in I_2 is computed from (5) and (6), and the procedure is repeated for the next time interval.

In order to facilitate the numerical calculation and the analytical study, in the following we use a normalized version of (4)–(6). We obtain such equations by combining (5) and (6), and by introducing the following normalized input parameters

$$\theta = RC/T \tag{7}$$
$$\Gamma = \frac{Z-R}{Z+R} = \frac{\zeta - 1}{\zeta + 1} \tag{8}$$
$$h_q = \frac{(\zeta - 1)Rm_q - 1}{(\zeta + 1)Rm_q + 1} \qquad q = -1, 0, 1 \tag{9}$$

where $\zeta = Z/R$. The parameter Γ is the reflection coefficient of the TL with respect to R (so that $|\Gamma| \leq 1$ for $\zeta \geq 0$) and h_q is a fundamental parameter for the case $C = 0$ [see (14)]. The normalized equations in the parameters $\{\theta, \Gamma, h_q, E\}$ write

$$\theta\frac{d}{d\tau}\tilde{v}(\tau) + \overline{\Lambda}_{Dq}[\tilde{v}(\tau) - E] + q(\overline{\Lambda}_{D0} - \overline{\Lambda}_{Dq})$$
$$= (1 - \Gamma)\left[\tilde{b}(\tau) - \frac{E}{2}\right], \qquad q = -1, 0, 1 \tag{10}$$
$$\cdot\, \tilde{b}(\tau + 1) = \Gamma\tilde{b}(\tau) - \frac{1}{2}(1 + \Gamma)\tilde{v}(\tau) \tag{11}$$

where

$$\overline{\Lambda}_{Dq} = \frac{1}{2}\,\frac{1 - \Gamma^2}{\Gamma - h_q} \tag{12}$$

and

$$\tau = t/T. \tag{13}$$

In these equations, the tilde indicates functions of the normalized time τ, and q is the index of the region of linear operation at time τ selected by the value of $\tilde{v}(\tau) - E$.

III. Overview of the Case $C = 0$

The TDCC with $C = 0$ has been detailedly studied in a series of papers (e.g., see [1], [2], [8]). In this section, we review its main features within the framework of (10) and (11). The reader is referred to Appendix I for proofs and discussions supporting the results here summarized.

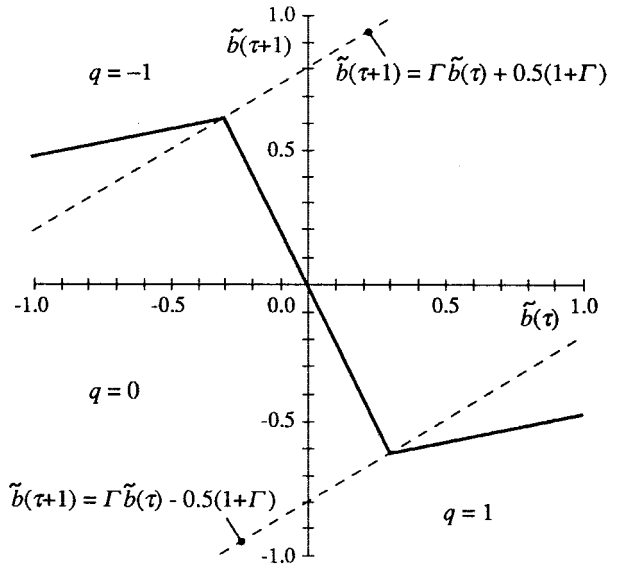

Fig. 3. Example of piecewise linear mapping describing the TDCC behavior. The function represented is obtained for $h_0 = -2$, $h_1 = 0.2$, $\Gamma = 0.6$.

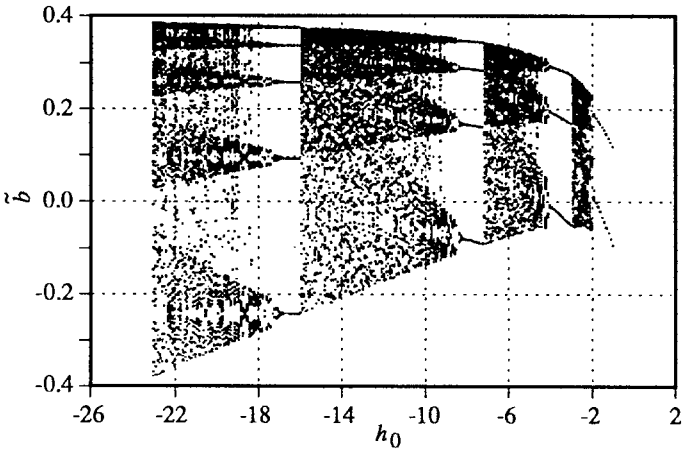

Fig. 4. Bifurcation diagram showing the period-adding phenomenon for $\theta = 0$. The bifurcation parameter is h_0; the other parameters are: $h_1 = 0.49$, $\Gamma = 0.6$, $E = 0.78$.

If $C = 0$, i.e., $\theta = 0$, the differential term of (10) vanishes and $\tilde{v}(\tau)$ becomes an algebraic function of $\tilde{b}(\tau)$. In this case, (10) and (11) can be reduced to a nonlinear first-order difference equation, i.e., a mapping whose properties are responsible of the system dynamics.

The family of mappings for the circuit variable $\tilde{b}(\tau)$, i.e., Φ: $\tilde{b}(\tau) \rightarrow \tilde{b}(\tau+1)$, is reported here in the case $E = 0$:

$$\tilde{b}(\tau+1) = h_q\tilde{b}(\tau) + \Delta h_q, \qquad q = -1, 0, 1 \tag{14}$$

where

$$\Delta h_q = \frac{1}{2}\,\frac{1+\Gamma}{\Gamma - h_0}(h_0 - h_q)q.$$

In the above equation, $q = 0$ holds for $|\tilde{b}(\tau)| \leq |b_0|$,with $b_0 = (1/2)\,(1+\Gamma/\Gamma - h_0)$; $q = -1$ holds for $\tilde{b}(\tau) < -b_0$ if $b_0 > 0$ and for $\tilde{b}(\tau) > -b_0$ if $b_0 < 0$; $q = 1$ holds for $\tilde{b}(\tau) > b_0$ if $b_0 > 0$ and for $\tilde{b}(\tau) < b_0$ if $b_0 < 0$. It is useful to remark that the slopes of the mapping Φ coincide with the h_q parameters.

A member of the family (14) is shown in Fig. 3, along with the boundaries dividing the plane $(\tilde{b}(\tau), \tilde{b}(\tau+1))$ in the three regions of linear operation. The stability properties of the fixed points of (14) (i.e., those points satisfing $\tilde{b}(\tau+1) = \tilde{b}(\tau)$) show that for $|\Gamma| < 1$ (and $E = 0$) no chaotic behavior can be obtained for any value of h_q [10] (see Appendix I).

A chaotic behavior of the TDCC with $C = 0$ has been shown in [1] by introducing the voltage generator E. Such a generator breaks the symmetry of the mappings (14), by dragging them of a quantity $E/2$ along the $\tilde{b}(\tau)$ axis and $-E/2$ along the $\tilde{b}(\tau+1)$ axis. In this way, mappings of the type of Fig. 3 can be converted into the mapping shown in [1, Fig. 10], which leads to the period-adding phenomenon described in [1] and shown in a particular case in Fig. 4.

Other chaotic families of mappings can be obtained from the TDCC with $C = 0$ and $E = 0$ by slight modifications. As example, the family of canonical tent functions can be obtained by proper negative values of R (see Appendix I). For the sake of simplicity, in what follows, we suppose the normalized TL impedance ζ to be positive, so that always we have $|\Gamma| < 1$.

IV. TDCC WITH CAPACITOR

The behavior of the TDCC is strongly influenced by the presence of the capacitor. If $C \neq 0$, $\tilde{v}(\tau)$ is a state variable, solution of the first order differential equation (10) having $\tilde{b}(\tau)$ as the source term, and the whole problem is of differential-difference type. In particular, (10) and (11) can be reduced to a first order nonlinear differential-difference equation of neutral type [10], which may be of some help in the circuit study.

General results are scarcely available for problems of this kind [1], [11], [13]. In fact, owing to the infinite dimension of the state space, the dynamics of the above equations is unlikely to be described by analytical methods and by standard techniques developed for finite dimensional systems (e.g., Poincaré maps, detection of homoclinic and heteroclinic orbits, etc.). There are, however, two simple tools for a qualitative study of the dynamics of such a system: the detection of the equilibrium points with the analysis of their stability, and extensive numerical simulations.

The equilibrium points are independent of C and are obtained in the usual way by intersecting the 1-D mapping Φ: $\tilde{b}(\tau) \rightarrow \tilde{b}(\tau+1)$ with the straight line $\tilde{b}(\tau+1) = \tilde{b}(\tau)$.

For $C = 0$, since the dynamics of the system is completely described by the mapping Φ, the stability properties of the equilibrium points follow directly from the slopes h_q of the mapping Φ (see Appendix I).

When the capacitor is added, the equilibrium points do not change, but their stability properties may vary. In fact, in the dynamical case, such properties are determined by the characteristic frequencies Λ_{kq} of the circuit in each region of linearity q.

The characteristic frequencies, hereafter called eigenvalues, are solutions of the characteristic equation below, which is obtained from (10) and (11) by eliminating every source term and looking for a solution of the form $\tilde{b}(\tau) = b_o \exp(\Lambda\tau)$, $\tilde{v}(\tau) = v_o \exp(\Lambda\tau)$, where b_o and v_o are constants and $\Lambda = \Lambda_r + j\Lambda_i$.

$$e^{\Lambda}(\Lambda + \Lambda_{Dq}) = \Gamma(\Lambda + \Lambda_{Nq}) \tag{15}$$

where

$$\Lambda_{Dq} = \overline{\Lambda}_{Dq}/\theta, \quad \Lambda_{Nq} = h_q \Lambda_{Dq}/\Gamma. \tag{16}$$

The above equation has infinitely many roots and it can be shown that it defines a set of eigenfunctions which represents the solution of (10) and (11) completely (see Appendix II).

A. Solution of the Characteristic Equation

A direct parametric analysis of the eigenvalue location is prevented by the lack of an analytical expression for the roots of (15). In order to gain some insight into the effects of the parameter values, we have found the regions of the parameter space where the circuit is stable, i.e., where all the eigenvalues have negative real part. Then, this stability map is used as a guide for a numerical study of the eigenvalue distributions as the parameter space $\{\theta, h_q, \Gamma\}$ is explored.

In such a parameter space, $C = 0$ corresponds to $\theta = 0$; in this case the stability of the fixed points follows from the h_q values.

For $C \neq 0$ the stability regions can be determined by resorting to [11, Theorems 13.7 and 13.3], originally stated by Pontrjagin. Such theorems give a set of conditions that has to be verified in order that all the roots of a polynomial $P(z, \exp(z))$ have negative real part; the application of such results to (15) is not trivial and requires a lengthy proof (summarized in Appendix III and reported in [14]), which leads to the following proposition:

Proposition 1: In each linear region $\mathcal{R}_q$, all the roots of (15) with $|\Gamma| < 1$ have negative real part iff, for any given value of Γ, parameters h_q and θ satisfy $h_q > 1$ and $\theta > \theta_1(h_q)$, or $-1 < h_q < \Gamma$, or $h_q < -1$ and $\theta > \theta_2(h_q)$, where the curves θ_1 and θ_2 have the following parametric equation:

$$\theta = \frac{\sin y}{2(\Gamma - y\cos y)} \frac{1-\Gamma^2}{\Gamma - h_q}$$
$$h_q = \frac{1 - \Gamma\cos y}{\cos y - \Gamma} \tag{17}$$

and are defined for different ranges of the parameter y:

$$\theta_1 : 0 \leq y < \arccos\Gamma \tag{18}$$
$$\theta_2 : \arccos\Gamma < y < \pi. \tag{19}$$

Two examples of stability maps for two different Γ values are shown in Fig. 5, where points in the dashed areas represent parameter values leading to stable eigenvalues. The value of Γ affects the aspect of the maps, as Fig. 5 shows, but not their structure, which is always composed of two stable areas: one above the level $h_q = +1$ and one below the level $h_q = \Gamma$. Additional characteristic elements of the stability maps are the abscissae $\theta_0 = (1+\Gamma)/2(1-\Gamma$ (where the θ_1 curve intersects the $h_q = +1$ boundary) and $\theta_v = (1/2)\sqrt{1-\Gamma^2}/\arccos\Gamma)$ (the vertical asymptote of θ_1 and θ_2).

The stability map offers a first insight into the effects of the capacitor. For $\theta = 0$ (i.e., $C = 0$), the stable region is composed of the segment $|h_q| < 1$ on the h_q axis. When θ takes a finite, nonzero value, the point representing the circuit parameters leaves the h_q axis and enters the (θ, h_q) plane. Fig. 5 shows that, in this transition, an equilibrium point remains stable if $-1 < h_q < \Gamma$, remains unstable (i.e., at least one eigenvalue has positive real part) if $|h_q| \geq 1$, and switches from a stable to an unstable state if $\Gamma \leq h_q < 1$. It is worth remarking that the jump from stable to unstable state happens for any arbitrary small θ. Furthermore, a transition from unstable to stable state can be obtained for $|h_q| \geq 1$ by large enough capacitors (i.e., by large enough θ values), whereas the equilibrium point remains unstable for any positive value of θ if $\Gamma \leq h_q < 1$. As a conclusion, the stability map highlights how the introduction of the capacitor C in the TDCC can completely change its dynamics and points out the importance of parasitic C values for particular combinations of h_q and Γ. More details will be given in the next section.

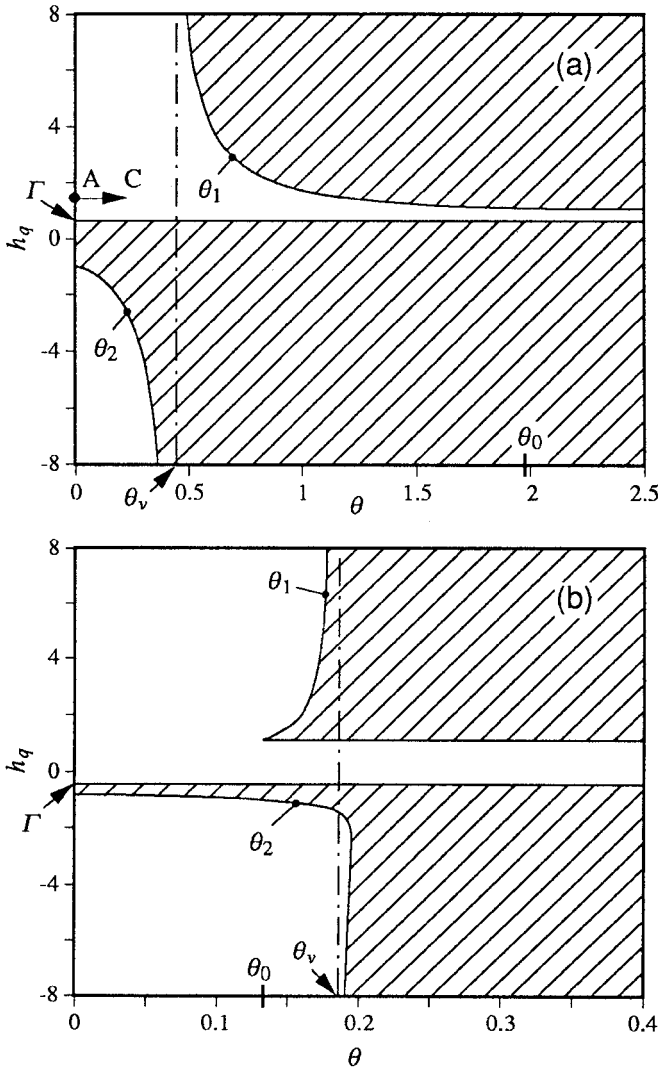

Fig. 5. Stability map in (θ, h_q) plane: (a) for $\Gamma = 0.6$. (b) for $\Gamma = -0.58156$. In the dashed regions all the eigenvalues have negative real part, whereas outside there exists at least one eigenvalue with positive real part.

Further information on the eigenvalue distribution can be obtained by the numerical computation of eigenvalues. We base our numerical procedure on the modulus and phase conditions arising from (15), because their graphic representation

allows also qualitative predictions of the eigenvalue location for entire portions of the parameter space. Such conditions are

$$\begin{aligned} &e^{2\Lambda_r}[(\Lambda_r+\Lambda_{Dq})^2+\Lambda_i^2]=\Gamma^2[(\Lambda_r+\Lambda_{Nq})^2+\Lambda_i^2] \\ &\Lambda_i+\arg\{\Lambda_r+\Lambda_{Dq}+j\Lambda_i\}=\arg\{\Gamma\} \\ &\qquad+\arg\{\Lambda_r+\Lambda_{Nq}+j\Lambda_i\}+2k\pi \\ &\qquad k=\cdots,-1,0,1,2,\cdots. \end{aligned} \tag{20}$$

The modulo condition states that, for any Λ_r value, the possible roots can have only the following values of their imaginary part Λ_i:

$$f_1(\Lambda_r)=\pm\sqrt{\frac{\Gamma^2(\Lambda_r+\Lambda_{Nq})^2-(\Lambda_r+\Lambda_{Dq})^2e^{2\Lambda_r}}{e^{2\Lambda_r}-\Gamma^2}}. \tag{21}$$

A second locus of possible Λ_i values is obtained by replacing (21) into the phase condition:

$$\begin{aligned} f_{2k}(\Lambda_r)=&-\arg\{\Lambda_r+\Lambda_{Dq}+jf_1(\Lambda_r)\} \\ &+\arg\{\Gamma\}+\arg\{\Lambda_r+\Lambda_{Nq}+jf_1(\Lambda_r)\}+2k\pi, \\ &k=\cdots,-1,0,1,2,\cdots. \end{aligned} \tag{22}$$

The intersections of $f_1(\Lambda_r)$ and $f_{2k}(\Lambda_r)$ give the roots Λ_{kq} of (15). They can be extimated graphically and, if needed, refined by a suitable numerical method.

The graphic analysis of curves $f_1(\Lambda_r)$ and $f_{2k}(\Lambda_r)$ shows that there are 10 different types of eigenvalue distributions, which hold in 10 regions of the parameter space [14]. These regions are listed in Table I, along with the corresponding qualitative loci of eigenvalues as θ is varied. In Table I, dots indicate the eigenvalue locations for $\theta \ll 1$ and arrows show the trajectories of eigenvalues as θ is increased.

The eigenvalue distributions for $\theta = 0$ can be easily obtained from (15), which simplifies to $\exp(\Lambda)=h_q$. Thus, $f_1(\Lambda_r)$ is the vertical line $\Lambda_r=\ln(|h_q|)$, and $f_{2k}(\Lambda_r)$ is the horizontal line $\Lambda_i=\arg\{h_q\}+2k\pi$. The eigenvalues Λ_{kq} lie on the vertical line, spaced of 2π and simmetrically located with respect to the Λ_r axis. A real Λ_{kq} exists only if $h_q \geq 0$ whereas all the eigenvalues have negative (non-negative) real part if $|h_q|<1$ ($|h_q| \geq 1$).

For $\theta \neq 0$, $f_1(\Lambda_r)$ becomes the curve described by (21). It exists only where $f_1^2(\Lambda_r)$ is non-negative, has a vertical asymptote at $\Lambda_{rv}=\ln(|\Gamma|)<0$ and is composed of a main branch (evolution of the vertical line for the $\theta = 0$ case, which bends toward the Λ_{rv} asymptote) and, possibly, minor branches located around $-\Lambda_{Dq}$ and $-\Lambda_{Nq}$. A numerical example of the evolution of the $f_1(\Lambda_r)$ curve and of the eigenvalue locations for $\Gamma=0.6$, $h_q=1.5$ and θ varying from $\theta = 0$ to $\theta = 0.21$ is given in Fig. 6. The parameter values of this example lie on the path A-C on the stability map of Fig. 5(a) and the eigenvalue distribution obtained corresponds to type VI of Table I.

The stability map and Table I provide a detailed qualitative knowledge of the eigenvalue location for the whole parameter space, allowing to identify the parameter values for which interesting dynamical behaviors are most likely to occur. As an example, they point out that the transition from stable to unstable configuration by crossing of θ_1 (i.e., $h_q>1$, types I or VI of Table I) or θ_2 (i.e., $h_q<-1$, types V or X of Table I)

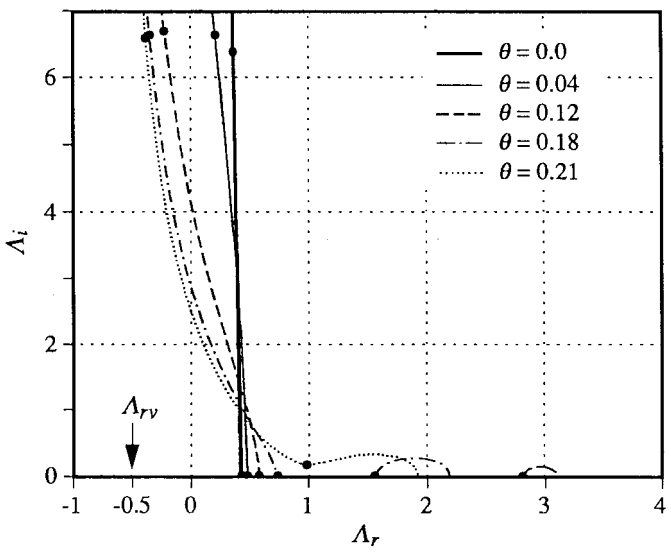

Fig. 6. $f_1(\Lambda_r)$ curves (lines) and some of the eigenvalues (solid circles) for $\Gamma = 0.6$, $h_q = 1.5$ and $\theta = 0.0, 0.04, 0.12, 0.18, 0.21$, corresponding to points on the path A-C of Fig. 5(a). The $f_1(\Lambda_r)$ minor branch of the $\theta = 0.04$ case does not appear because it is located for $\Lambda_r \gg 4$, whereas at $\theta = 0.21$ the minor branch has just joined the main one.

is due to a couple of complex conjugate eigenvalues shifting in the right half plane, or that the unstable behavior of region $\theta>0$ and $\Gamma \leq h_q \leq 1$ (i.e., types II or III or VII of Table I) is due to a positive real eigenvalue. It turns out that this real eigenvalue is proportional to $-\Lambda_{Dq}$ and hence to $1/\theta$; in this case, therefore, the smaller is the capacitance, the stronger is the instability of the equilibrium and the presence of any parasitic capacitance cannot be neglected at all.

B. Qualitative Analysis and Simulation Results

The knowledge of the stability map and of the eigenvalue distribution in each region of linearity (see Fig. 5 and Table I) allows us to perform a qualitative analysis of the dynamical behavior of the TDCC.

Mainly there are two things of interest: the behavior for a generic $\theta>0$ and that for small values of θ, in order to evaluate the effects of parasitics on the dynamics of the difference equation, which describes the circuit for $\theta = 0$.

First, we consider the case of a generic $\theta>0$. As shown in Appendix II, the solution $\tilde{v}(\tau)$ in each region of linearity can be expressed as the sum of two terms, associated to real and complex eigenvalues, respectively. For generic initial conditions, each of these contributions is mainly influenced by the eigenvalues with the largest real part, that for this reason will be called *dominant eigenvalues*.

In particular, we define the set of the *dominant* eigenvalues as the set composed by all the eigenvalues Λ_d satisfying any of the following two conditions:

- if Λ_d is real, then $\Lambda_d \geq \Lambda_{rk}\ \forall k$, where Λ_{rk} is a generic real eigenvalue;
- if Λ_d is complex with a finite imaginary part, then $\mathrm{Re}[\Lambda_d] \geq \mathrm{Re}[\Lambda_{ik}]\ \forall k$, where Λ_{ik} is a generic complex eigenvalue.

Table I shows that regions $\mathcal{R}_0$ and $\mathcal{R}_{\pm 1}$ may exhibit 10 different eigenvalue distributions, 5 for $\Gamma<0$ and 5 for $\Gamma>0$,

TABLE I

TYPES OF EIGNEVALUE DISTRIBUTIONS. THE DISTRIBUTIONS ARE QUALITATIVELY REPRESENTED IN THE PLOTS, WHERE SOLID CIRCLES INDICATE THE EIGENVALUE LOCATIONS IN THE UPPER HALF Λ PLANE FOR A SMALL θ VALUE, THE ARROWS INDICATE THE EIGENVALUE TRAJECTORIES FOR GROWING θ AND THE DASHED VERTICAL LINES REPRESENT THE Λ_{rv} ASYMPTOTES

$\{\Lambda_{kq}\}$ at $\theta << 1$ (dots) and their trajectories for growing θ	Remarks	$\{\Lambda_{kq}\}$ at $\theta << 1$ (dots) and their trajectories for growing θ	Remarks
I $\Gamma < 0$ and $h_q > 1$ 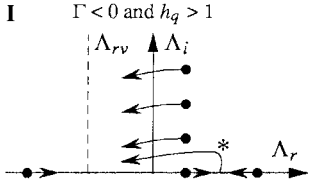	the star indicates the last eigenvalue crossing the Λ_i axes	**VI** $\Gamma > 0$ and $h_q > 1$ 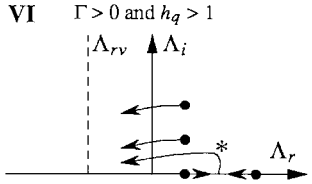	the star indicates the last eigenvalue crossing the Λ_i axes
II $\Gamma < 0$ and $\lvert\Gamma\rvert < h_q < 1$ 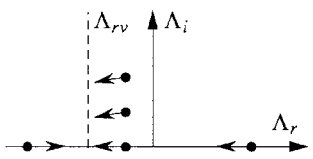	the real positive eigenvalue never crosses the Λ_i axes and reaches the origin for $\theta = \infty$	**VII** $\Gamma > 0$ and $\Gamma < h_q < 1$ 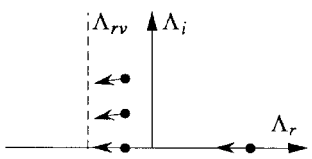	the real positive eigenvalue never crosses the Λ_i axes and reaches the origin for $\theta = \infty$
III $\Gamma < 0$ and $\lvert h_q\rvert < \lvert\Gamma\rvert$ 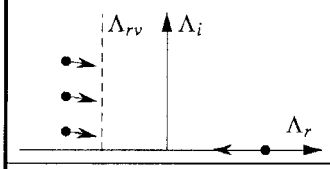	the real positive eigenvalue never crosses the Λ_i axes and reaches the origin for $\theta = \infty$	**VIII** $\Gamma > 0$ and $0 < h_q < \Gamma$ 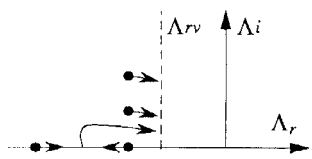	always stable
IV $\Gamma < 0$ and $-1 < h_q < \Gamma$ 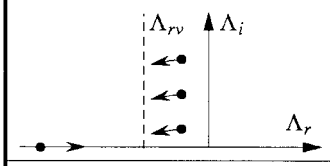	always stable	**IX** $\Gamma > 0$ and $-1 < h_q < 0$ 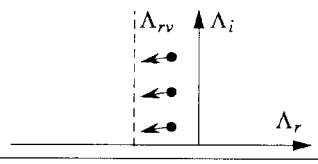	always stable
V $\Gamma < 0$ and $h_q < -1$ 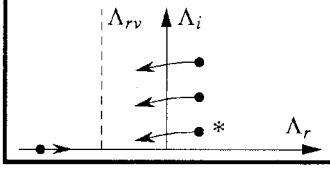	the star indicates the last eigenvalue crossing the Λ_i axes	**X** $\Gamma > 0$ and $h_q < -1$ 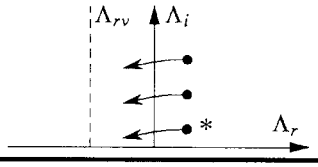	the star indicates the last eigenvalue crossing the Λ_i axes

respectively. Since Γ is a global parameter, an exhaustive examination of the dynamic behavior would require to consider 50 cases. We will restrict our discussion to some examples, with the purpose of showing that the TDCC dynamics can be qualitatevely studied by taking into account the stability map (similar to those of Fig. 5), the eigenvalue distributions reported in Table I and the dominant eigenvalues, computed as described in Section IV-A.

In particular, we concentrate on the chaotic behavior of the TDCC. We will show that bifurcation processes and strange attractors similar to those occurring in the classical Chua's circuit (CC) [15] can be obtained if the dominant eigenvalue distribution of the TDCC is close to the eigenvalue distribution of the CC in each region of linearity.

It is known (see [15]) that a CC, which exhibits a period doubling bifurcation process leading to chaos, presents the following properties:

a) in each linear region there exists an equilibrium point;
b) in the outer regions there are one negative real eigenvalue and a pair a complex eigenvalues whose real part, originally negative, becomes positive by varying a bifurcation parameter, i.e., a Hopf-bifurcation (in the sense explained in [16]) occurs;
c) in the central region there are one positive real eigenvalue and two complex eigenvalues with negative real part.

The use of stability maps (like those of Fig. 5) and of Table I allows us to recognize when a similar situation may occur in the case of the TDCC.

From Table I it turns out that if $\Gamma > 0$, there are no values of h_q satisfying the condition b).

On the other hand, if $\Gamma < 0$ and $|h_q| > 1$, the stability map [e.g., Fig. 5(b)] and Table I (cases I and V) show that the condition b) is satisfied in $\mathcal{R}_q$ for suitable values of θ. In fact:

- there exists a value $\theta = \theta_{hp}$ which corresponds to a Hopf-bifurcation, i.e., such that all the roots of the characteristic equation (15) have negative real part, with the exception of a pair of imaginary eigenvalues, which are dominant. This value of θ may be computed through (17), after choosing a value for Γ and $h_{\pm 1}$.

TABLE II
DOMINANT EIGENVALUES AND DYNAMIC BEHAVIOR OF THE TDCC FOR $h_0 = 0.358275, h_{\pm 1} = -4.90733$ AND $\Gamma = -0.58156$

	Dominant Eigenvalues		
θ	$\mathcal{R}_0$	$\mathcal{R}_{\pm 1}$	*Dynamic behavior*
0.18	$\lambda_1 = 1.63373$	$\lambda_1 = -3.41716$	Period-1 limit cycle
	$\lambda_{23} = -1.09964 \pm j2.13018$	$\lambda_{23} = 0.0508564 \pm j2.34353$	
0.1725	$\lambda_1 = 1.7338$	$\lambda_1 = -3.59282$	Period-2 limit cycle
	$\lambda_{23} = -1.13699 \pm j2.09662$	$\lambda_{23} = 0.083246 \pm j2.34133$	
0.169	$\lambda_1 = 1.78358$	$\lambda_1 = -3.67931$	Period-4 limit cycle
	$\lambda_{23} = -1.15554 \pm j2.08035$	$\lambda_{23} = 0.0987297 \pm j2.34064$	
0.16850	$\lambda_1 = 1.79086$	$\lambda_1 = -3.69191$	Spiral attr.
	$\lambda_{23} = -1.15825 \pm j2.07799$	$\lambda_{23} = 0.100962 \pm j2.34056$	
0.16830	$\lambda_1 = 1.79378$	$\lambda_1 = -3.69697$	Periodic window
	$\lambda_{23} = -1.15933 \pm j2.07705$	$\lambda_{23} = 0.101855 \pm j2.34052$	
0.165	$\lambda_1 = 1.84304$	$\lambda_1 = -3.78197$	Double Scroll attr.
	$\lambda_{23} = -1.17765 \pm j2.06125$	$\lambda_{23} = 0.11672 \pm j2.34011$	
0.1644	$\lambda_1 = 1.85221$	$\lambda_1 = -3.79774$	Periodic window
	$\lambda_{23} = -1.18105 \pm j2.05834$	$\lambda_{23} = 0.119445 \pm j2.34006$	
0.1635	$\lambda_1 = 1.86608$	$\lambda_1 = -3.82158$	Double Scroll attr.
	$\lambda_{23} = -1.1862 \pm j2.05394$	$\lambda_{23} = 0.123548 \pm j2.33999$	

- for values of θ close to θ_{hp} there is only one real eigenvalue, that therefore is also dominant; such an eigenvalue is negative.

Moreover, if $\Gamma < 0$, in cases II and III of Table I the condition c) is satisfied: in fact, in these cases, any generic region $\mathcal{R}_q$ exhibits one positive real eigenvalue (that is dominant), whereas all the other eigenvalues have negative real part (and among them there is a pair of complex dominat eigenvalues).

The above considerations suggest that for reproducing a dominant eigenvalue distribution satisfying the above conditions b) and c), it is convenient to choose $\Gamma, h_{\pm 1}$, and h_0 in such a way that case I or V of Table I holds for $\mathcal{R}_{\pm 1}$, whereas case II or III holds for $\mathcal{R}_0$.

As a first example, we have chosen a TDCC strictly related to the CC of Fig. 1 of [15], whose dynamics has been studied in great details in several papers. The lumped elements of the TDCC have been fixed to the same values of those of the considered CC, i.e., $C = 1/9, G = 10/7$, $m_0 = -0.8, m_1 = -0.5$. Thus, the two circuits have the same equilibrium values of the capacitor voltage and, hence, condition a) is verified. The TL characteristic impedance is assumed equal to $Z = \sqrt{L/C_2} = 1/\sqrt{7}$, being L and C_2, respectively, the inductance and the second capacitance used in [15]. This choice, in terms of the parameters h_q and Γ yields $h_0 = 0.358\,275$, $h_{\pm 1} = -4.907\,33$, and $\Gamma = -0.581\,56$; θ is the bifurcation parameter.

The eigenvalue distributions in $\mathcal{R}_{\pm 1}$ and $\mathcal{R}_0$ are of type V and III, respectively, according to the previous considerations. The value of θ which gives rise to the Hopf-bifurcation in regions $\mathcal{R}_{\pm 1}$ can be analytically computed through (17) and turns out to be $\theta_{hp} = 0.192\,302\,79$. In Table II we have reported the TDCC dominant eigenvalue for some values of θ, lying in the left neighborhood of θ_{hp}: as expected they satisfy the conditions b) and c) listed above.

In order to perform a detailed comparison, we have reported the eigenvalues of the considered CC in Table III assuming C_1 (see [15, Fig. 1]) as bifurcation parameter.

Tables II and III show that not only the TDCC and the CC eigenvalue distributions are close, but also that they move according to similar rules, when the bifurcation parameters are varied. In fact by decreasing θ in the TDCC (or C_1 in the CC) we observe that:

- in all the regions the absolute value of the real (imaginary) part of the complex eigenvalues increases (decreases);
- in the central region $\mathcal{R}_0$ the positive real eigenvalue increases whereas in the outer regions $\mathcal{R}_{\pm 1}$ the negative real eigenvalue decreases.

The simulation of the TDCC has been performed by using a Runge-Kutta algorithm with fixed step and starting from a constant initial condition of the type $\tilde{v}(0) = 0.1$ V and $\tilde{b}(\tau) = 0, \tau \in]0, 1]$. The results are reported in Fig. 7 and 8 and confirm that, owing to the distribution of its dominant eigenvalues, the TDCC exhibits a period-doubling route to chaos and a sequence of strange attractors similar to those observed in the classical CC. In fact:

- for $\theta > \theta_{hp}$ the two equilibrium points located in $\mathcal{R}_{\pm 1}$ are stable; the equilibrium point in $\mathcal{R}_0$ is unstable because

TABLE III
EIGENVALUES AND DYNAMIC BEHAVIOR FOR THE CLASSICAL CHUA'S CIRCUIT OF FIG. 1 OF [15] WITH $L = 1/7$, $C_2 = 1$, $G = 0.7$, $m_0 = -0.5$ AND $m_1 = -0.8$

	Eigenvalues		
C_1	$\mathcal{R}_0$	$\mathcal{R}_{\pm 1}$	*Dynamic behavior*
0.125	$\lambda_1 = 1.3396$	$\lambda_1 = -2.4509$	Period-1 limit cycle
	$\lambda_{23} = -0.61978 \pm j1.9484$	$\lambda_{23} = 0.0754 \pm j2.136$	
0.120	$\lambda_1 = 1.4107$	$\lambda_1 = -2.5554$	Period-2 limit cycle
	$\lambda_{23} = -0.63866 \pm j1.9306$	$\lambda_{23} = 0.094353 \pm j2.1346$	
0.1185	$\lambda_1 = 1.4331$	$\lambda_1 = -2.5881$	Period-4 limit cycle
	$\lambda_{23} = -0.64462 \pm j1.9252$	$\lambda_{23} = 0.10016 \pm j2.1342$	
0.117	$\lambda_1 = 1.4561$	$\lambda_1 = -2.6215$	Spiral attr.
	$\lambda_{23} = -0.65072 \pm j1.9197$	$\lambda_{23} = 0.10604 \pm j2.1338$	
0.116618	$\lambda_1 = 1.4621$	$\lambda_1 = -2.6301$	Periodic window
	$\lambda_{23} = -0.65223 \pm j1.9183$	$\lambda_{23} = 0.10755 \pm j2.1337$	
0.113	$\lambda_1 = 1.5204$	$\lambda_1 = -2.7140$	Double Scroll attr.
	$\lambda_{23} = -0.66770 \pm j1.9049$	$\lambda_{23} = 0.12203 \pm j2.1331$	

TABLE IV
DOMINANT EIGENVALUES AND DYNAMIC BEHAVIOR OF THE TDCC FOR $h_0 = 0.358275, h_{\pm 1} = 5$ AND $\Gamma = -0.58156$

	Dominant Eigenvalues		
θ	$\mathcal{R}_0$	$\mathcal{R}_{\pm 1}$	*Dynamic behavior*
0.17	$\lambda_1 = 1.76914$	$\lambda_1 = -2.62869$	Period-1 limit cycle
	$\lambda_{23} = -1.15016 \pm j2.08504$	$\lambda_{23} = 0.045111 \pm j2.00222$	
0.167	$\lambda_1 = 1.81296$	$\lambda_1 = -2.69871$	Period-2 limit cycle
	$\lambda_{23} = -1.16647 \pm j2.07087$	$\lambda_{23} = 0.0650341 \pm j1.99613$	
0.164	$\lambda_1 = 1.85836$	$\lambda_1 = -2.77061$	Spiral attr.
	$\lambda_{23} = -1.18334 \pm j2.05639$	$\lambda_{23} = 0.0852714 \pm j1.99026$	
0.16125	$\lambda_1 = 1.90143$	$\lambda_1 = -2.83825$	Double Scroll attr.
	$\lambda_{23} = -1.19932 \pm j2.04283$	$\lambda_{23} = 0.104099 \pm j1.98508$	

of the positive real eigenvalue; therefore any trajectory converges toward one of the equilibria lying in $\mathcal{R}_{\pm 1}$.

- beyond the Hopf bifurcation $(\theta < \theta_{hp})$ a period-1 limit cycle appears [see Fig. 7(a), with $\theta = 0.18$];
- by further decreasing θ the system goes through a sequence of period doubling bifurcations [$\theta = 0.1725$, period-2 limit cycle, Fig. 7(b); $\theta = 0.169$, period-4 limit cycle, Fig. 7(c)], until a spiral-like attractor [Fig. 7(d)] is observed. Continuing in decreasing θ, several periodic windows appear, (one of them is reported in Fig. 8(a), $\theta = 0.1683$), and finally double-scroll like attractors (see Fig. 8(b), $\theta = 0.1650$, and Fig. 8(d), $\theta = 0.1635$) are found. As for Chua's circuit, between two successive double-scrolls, periodic windows are present, as shown in Fig. 8(c) $(\theta = 0.1644)$. This alternance of periodic windows and double-scroll like attractors continues until $\theta = 0.1465$; for lower values of θ all trajectories become unbounded.

It is worth noting that, with a finite value of θ, chaos is observed even in absence of the voltage source E; this is a major difference with respect to the static case $\theta = 0$, where chaos may occur only if a suitable voltage source E is added in series to the Chua's diode. Furthermore, if θ is set to zero, (i.e., if the capacitance vanishes), the circuit turns out to be described by a nonsingle valued mapping Φ. The presence of the capacitor (i.e., $\theta > 0$) causes the circuit to be described by the differential-difference equations (10) and (11), thereby implying the uniqueness of the solution.

As a second example, we assume $h_{\pm 1} = 5$, without varying the parameters h_0 and Γ, in such a way that in each region there exists an equilibrium point [condition a)] and that the eigenvalue distributions in $\mathcal{R}_{\pm 1}$ and $\mathcal{R}_0$ are of type I and III, respectively. By choosing θ as bifurcation parameter, the dominant eigenvalues are reported in Table IV: it is seen that they satisfy conditions b) and c) listed above, and that also in this case their distribution is close to that of the considered CC.

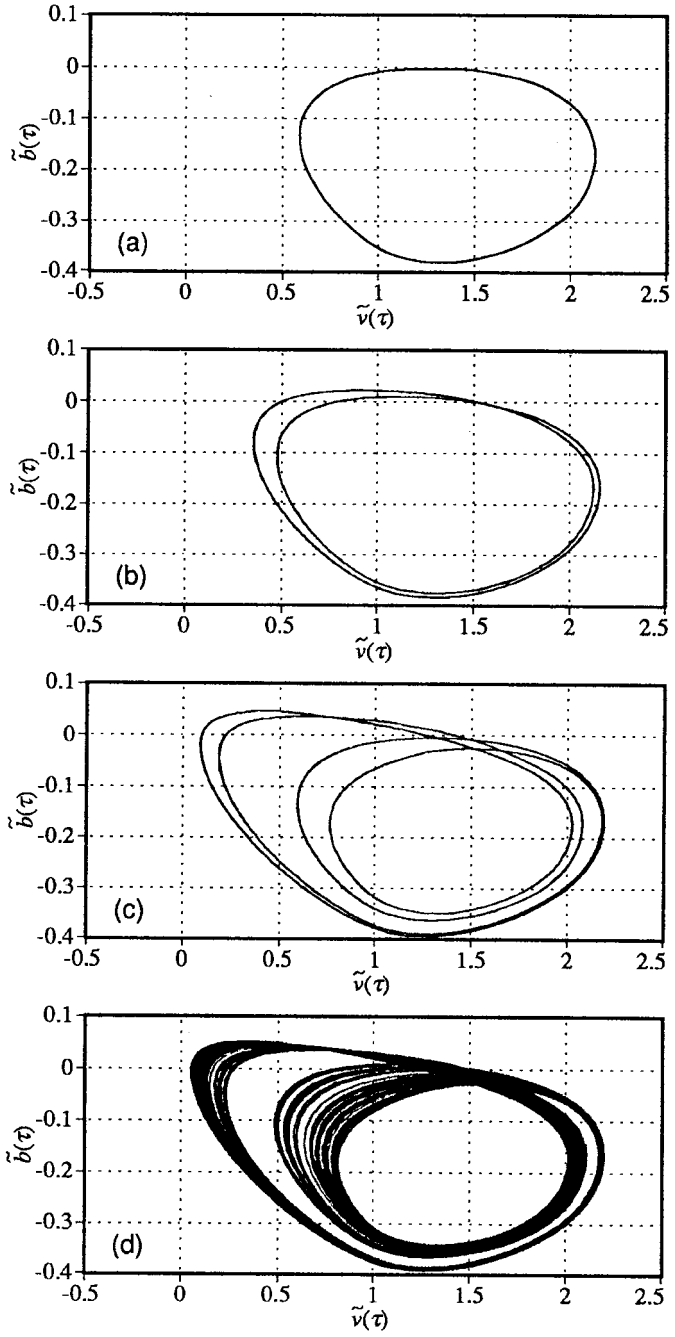

Fig. 7. Phase portrait of a period-doubling phenomenon. (a) Period-1 limit cycle ($\theta = 0.18$). (b) Period-2 limit cycle ($\theta = 0.1725$). (c) Period-4 limit cycle ($\theta = 0.169$). (d) Spiral attractor ($\theta = 0.1685$). The other parameters are $h_0 = 0.35828, h_1 = -4.9073, \Gamma = -0.58156$, and $E = 0$.

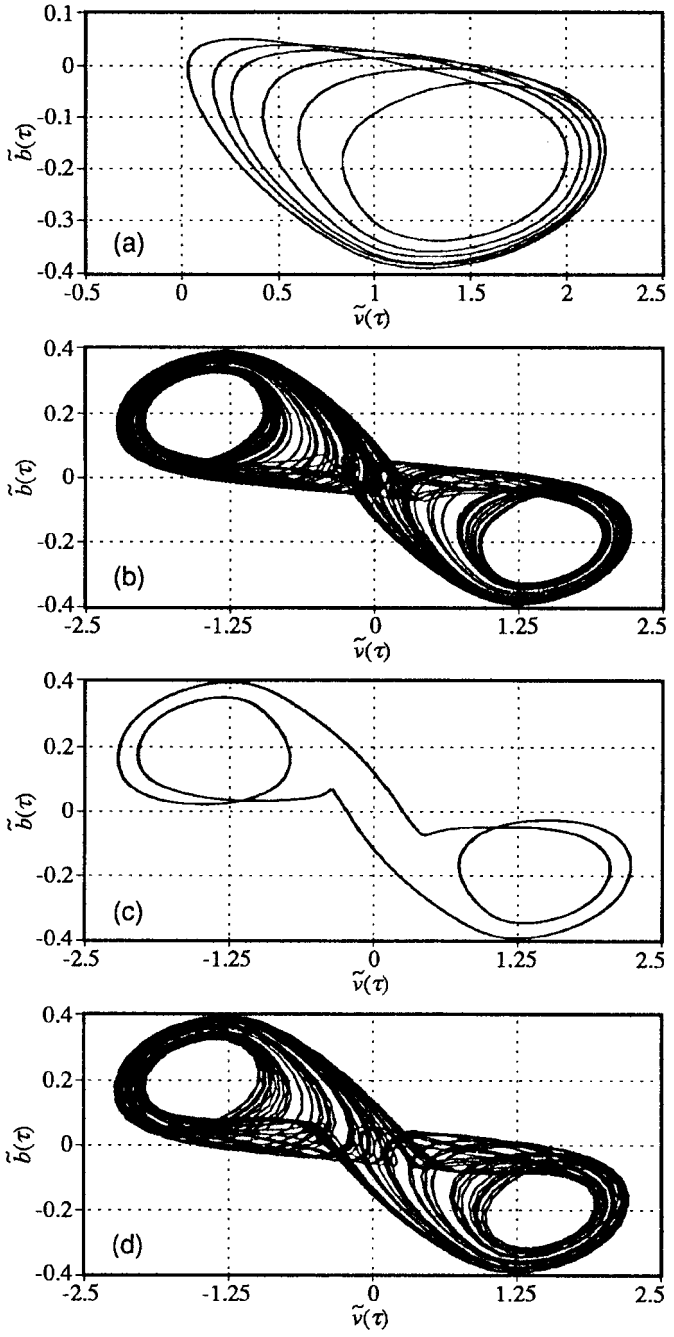

Fig. 8. Phase portrait of stable limit cycle windows in a chaotic region. (a) period 6 limit cycle ($\theta = 0.1683$). (b) Double scroll ($\theta = 0.165$. (c) $2-2$ window ($\theta = 0.1644$). (d) Double scroll ($\theta = 0.1635$). The other parameters are $h_0 = 0.35828, h_1 = -4.9073, \Gamma = -0.58156$, and $E = 0$.

The simulations shown in Fig. 9 confirm that, as expected, the TDCC exhibits a period-doubling route to chaos very similar to that previously observed.

Now let us turn our qualitative analysis to examine what happens when θ assumes very small positive values; this analysis may be of interest in assessing the effects of parasitics on the dynamics of the difference equation, which describes the circuit for $\theta = 0$.

Comparing the eigenvalue distributions reported in Table I with those for $\theta = 0$, it is apparent that in some cases there is a displacement of the eigenvalue distributions that can be considered a continuous function of θ. In these cases, it is reasonable to conjecture a continuous variation of the dynamics as θ appears. More precisely, we say that, in a region $\mathcal{R}_q$, the eigenvalue distribution for a small value of θ may be considered a continuous evolution of that corresponding to $\theta = 0$ if the eigenvalues Λ_k satisfy

$$\lim_{\theta \to 0^+} \mathrm{Re}[\Lambda_k] = \ln |h_q| \quad \forall k$$

except for a finite number of eigenvalues Λ_s such that

$$\lim_{\theta \to 0^+} \mathrm{Re}[\Lambda_s] = -\infty.$$

TABLE V
COMPARISON BETWEEN THE EIGENVALUE DISTRIBUTIONS AND THE DYNAMIC BEHAVIORS FOR $\theta = 0$ AND FOR SMALL θ'S. THE MEANING OF THE ACHRONIMA ARE THE FOLLOWING: C: CONTINUITY; CS: DISCONTINUITY WITH CHANGE OF SIGN OF THE REAL PART; NCS: DISCONTINUITY WITHOUT CHANGE OF SIGN OF THE REAL PART

Case		*eig. distribution*		*dynamic behavior*	
$\mathcal{R}_0$	$\mathcal{R}_{\pm 1}$	$\mathcal{R}_0$	$\mathcal{R}_{\pm 1}$	$\theta = 0$	*small* θ
$h_0 < \Gamma$	$h_{\pm 1} < \Gamma$	C	C	*similar dynamic behavior*	
$\Gamma < h_0 < 1$	$\Gamma < h_{\pm 1} < 1$	CS	CS	*one globally asymptotically stable equilibrium point, belonging either to* $\mathcal{R}_0$ *or to* $\mathcal{R}_{\pm 1}$*, depending on the value of* E	*unstable*
$\Gamma < h_0 < 1$	$h_{\pm 1} > 1$	CS	NCS	*locally stable if there exists one equilibrium point in* $\mathcal{R}_0$*; unstable otherwise*	*unstable*
$h_0 > 1$	$\Gamma < h_{\pm 1} < 1$	NCS	CS	*completely stable, with one or two stable equilibrium points belonging to* $\mathcal{R}_{\pm 1}$	*unstable*
$h_0 > 1$	$h_{\pm 1} > 1$	NCS	NCS	*unstable*	*unstable*

If the above conditions are not satisfied, we say that there is a discontinuity in the eigenvalue distribution as θ appears.

According to this definition and to Table I, cases IV, V, VIII, IX, and X are continuous, whereas cases I, II, III, VI, and VII are not. Note that the discontinuity is essentially due to the appearance of a large positive eigenvalue. If for $\theta = 0$ the eigenvalues have also positive real part, we say that the discontinuity takes place with no change of sign (NCS) in the real part; if this is not the case, the discontinuity is accompanied by a change of sign (CS) of the real part. As a consequence, cases I and VI are NCS-discontinuous, whereas cases II, III, and VII are CS-discontinuous.

The constraints (28) given in Appendix I for a single valued mapping restrict all the possible combinations of h_q values to those reported in Table V.

From this table it turns out that if a CS-discontinuity occurs in a region which exhibits a stable equilibrium point, then the dynamic behavior for small θ has an abrupt change with respect to the case $\theta = 0$ (see rows 2, 3, and 4). This fact has been confirmed through extensive simulations. On the contrary, for $h_0 < \Gamma$ and $h_{\pm 1} < \Gamma$ (see row 1 of Table V), since the eigenvalue distribution varies continuously with θ, we expect a similar dynamic behavior both for $\theta = 0$ and small θ. Such a conjecture has been verified by several simulations.

As an example we report the simulations that refer to the case $h_{\pm 1} = 0.49$, $\Gamma = 0.60$, $E = 0.78$ and h_0 within the interval $[-4, -1]$. For $\theta = 0$, as shown in Fig. 4, the system exhibits the period-adding phenomenon (see also [1, Fig. 11]).

By assigning a small value to θ, a similar succession of limit cycles, separated by chaotic regions, may be again observed as h_0 is varied. Of course, due to the small but *finite* value of θ, the extension of these regions may vary from that of the case $\theta = 0$. Assuming $\theta = 0.01$, the simulations of the TDCC show a limit cycle of period $\tau_0 = 2.2$ for $h_0 = -1.2$ [Fig. 10(a)]; decreasing h_0, a chaotic region is encountered and for $h_0 = -2.6$ the chaotic attractor of Fig. 10(b) is observed. A further decrease in h_0 reveals a new periodic window; Fig. 10(c) shows the limit cycle of period $2\tau_0 = 4.4$ obtained for $h_0 = -3.05$. Continuing in decreasing h_0, a new chaotic region appears [Fig. 10(d)].

As a concluding remark, we would like to point out that the result presented above is general. In fact, in [1] it is proved that the existence of the period-adding phenomenon requires $h_0 \leq -1$ and $0 \leq h_1 \leq 1$; since the single value mapping condition (28) holds and since $|\Gamma| < 1$, the condition of row 1 of Table V is satisfied, thereby implying the continuity of eigenvalue distributions. This would suggest that *any* TDCC which exhibits the period-adding phenomenon for $\theta = 0$, should present a similar dynamics even if a small capacitor is added to the circuit.

V. CONCLUSIONS

In this paper we have studied in details the effects of the presence of the capacitor on the dynamics of the TDCC. To this end, the circuit equations have been recasted in a normalized form, suitable for the investigation of the related characteristic equation in each region of linearity. By studying such an equation, the regions in the parameter space, where all the eigenvalues have negative real part, have been exactly determined, along with all the possible qualitative eigenvalue distributions.

For a finite value of C, this analysis has allowed to distinguish 10 different kinds of eigenvalue distributions in

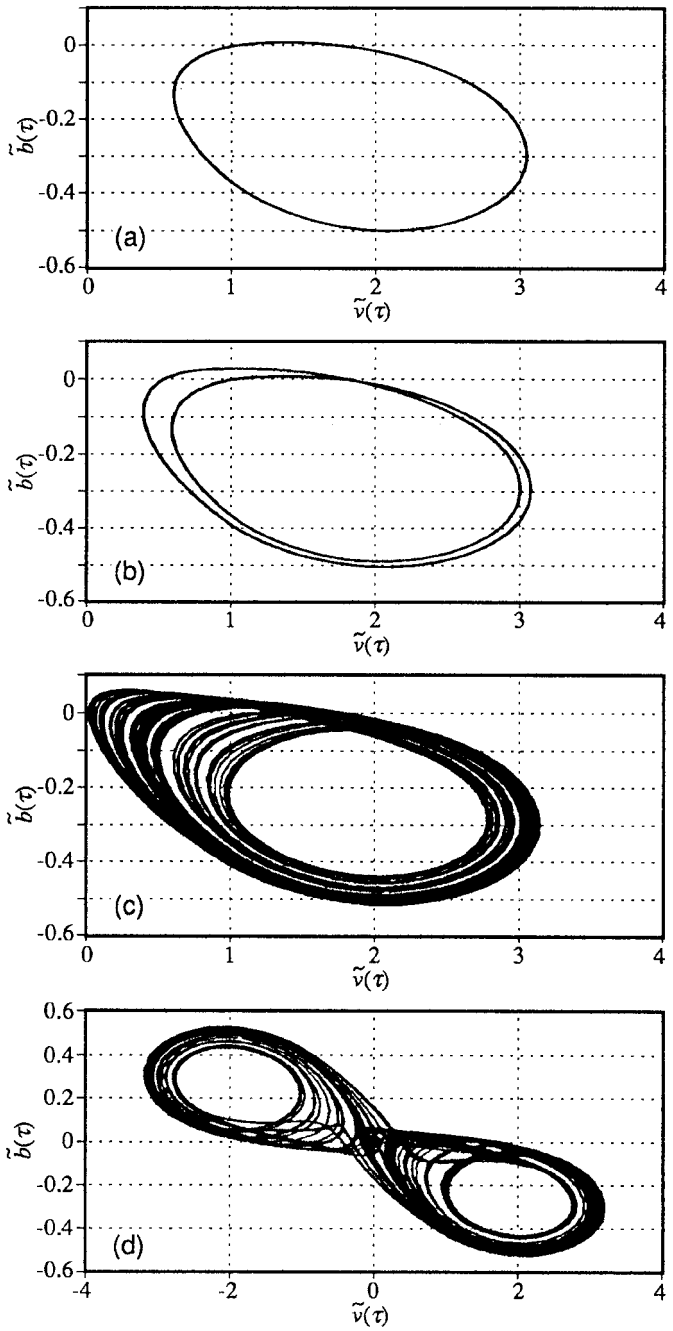

Fig. 9. Phase portrait of bifurcation process: (a) period-1 limit cycle ($\theta = 0.17$); (b) period-2 limit cycle ($\theta = 0.167$); (c) spiral attractor ($\theta = 0.164$); (d) double scroll ($\theta = 0.16125$). The other parameters are: $h_0 = 0.35828, h_1 = 5, \Gamma = -0.58156$ and $E = 0$.

each region of linearity, which give rise to 50 possible cases of different dynamic behaviors. Moreover, the analysis has shown that, in each region of linearity, the dynamics of this infinite dimensional system is mainly influenced by a finite set of eigenvalues, called dominant eigenvalues.

In order to test the validity of our qualitative analysis we have concentrated on a complex dynamic behavior: the occurrence of chaos. We have found that the TDCC may exhibit a bifurcation process and strange attractors similar to those occurring in the classical Chua's circuit if the dominant eigenvalue distribution of the TDCC is close to the eigenvalue

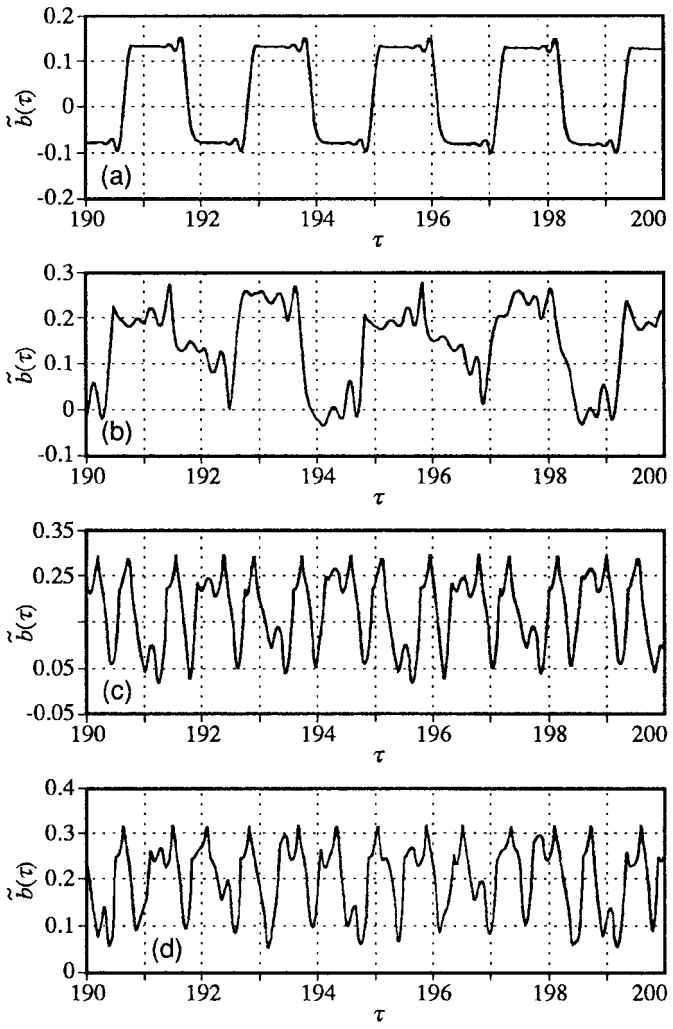

Fig. 10. Capacitor voltage versus time for $\theta = 0.01$, after a transient of 190. (a) $h_0 = -1.2$: periodic attractor of period $\tau_0 = 2.2$. (b) $h_0 = -2.6$: strange attractor. (c) $h_0 = -3.05$: periodic attractor of period $2\tau_0 = 4.4$. (d) $h_0 = -3.9$: strange attractor. The other parameters are $h_1 = 0.49$, $\Gamma = 0.60$, and $E = 0.78$.

distribution of the CC and if one (unstable) equilibrium point is present in each region of linearity. In contrast to the case $\theta = 0$, with a finite value of θ, this chaotic behavior is observed even in absence of the constant voltage source E.

For a small capacitor C (e.g., a parasitic element), we have shown that the behavior of TDCC may completely change if the eigenvalue distribution, in each region of linearity exhibiting a stable equilibrium point, does not approach that of the case $C = 0$. Furthermore, we have shown that, for the set of parameters giving rise to the period-adding phenomenon at $C = 0$, the eigenvalue distribution is continuous at $C = 0$ and, hence, it is reasonable to conjecture that the period-adding phenomenon still exists even if a *small* capacitor C is added to the circuit.

APPENDIX I

In this appendix, we derive and discuss the piecewise linear mappings which model the TDCC for $C = 0$. For the sake of generality, Γ may assume any real value in this Appendix.

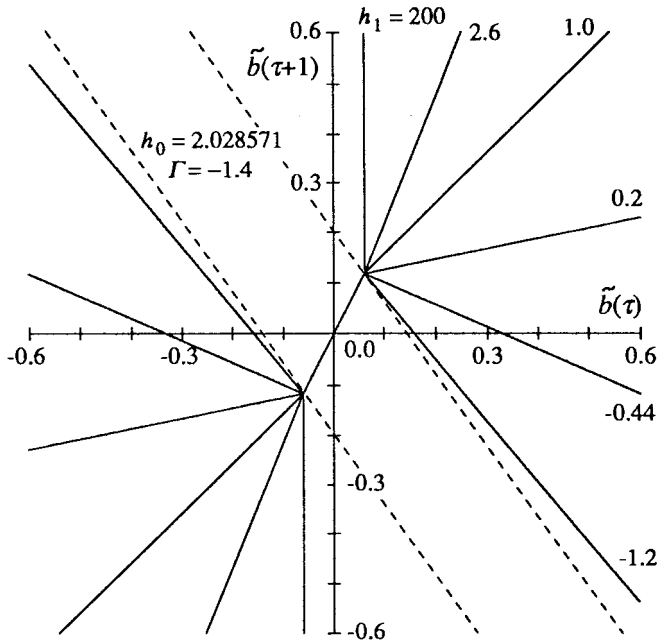

Fig. 11. Illustration of the graphic procedure to generate every possible piecewise linear mapping for the TDCC of Fig. 1. The fixed parameters are $h_0 = -2.028571$, $\Gamma = -1.4$.

It is expedient to start from the $E = 0$ case. For $C = 0$ and $E = 0$, (10) and (11) become

$$\overline{\Lambda}_{Dq}\tilde{v}(\tau) + q(\overline{\Lambda}_{D0} - \overline{\Lambda}_{Dq}) = (1-\Gamma)\tilde{b}(\tau) \qquad q = -1, 0, 1 \tag{23}$$

$$\tilde{b}(\tau+1) = \Gamma\tilde{b}(\tau) - \tfrac{1}{2}(1+\Gamma)\tilde{v}(\tau). \tag{24}$$

The mapping $\Phi_{h_0,h_1,\Gamma}$: $\tilde{b}(\tau) \to \tilde{b}(\tau+1)$ can be obtained by solving (23) for $\tilde{v}(\tau)$:

$$\tilde{v}(\tau) = \frac{1-\Gamma}{\overline{\Lambda}_{Dq}}\tilde{b}(\tau) - \frac{q(\overline{\Lambda}_{D0} - \overline{\Lambda}_{Dq})}{\overline{\Lambda}_{Dq}}. \tag{25}$$

Substituting (25) into (24), (14) of Section III is obtained

$$\begin{aligned}\tilde{b}(\tau+1) &= h_q\tilde{b}(\tau) + \Delta h_q,\\ \Delta h_q &= \frac{1}{2}\,\frac{1+\Gamma}{\Gamma - h_0}q(h_0 - h_q) \qquad q = -1, 0, 1\end{aligned} \tag{26}$$

where q is the index of the linear region where the circuit is operating.

In the plane $(\tilde{b}(\tau), \tilde{b}(\tau+1))$, regions $\mathcal{R}_q$ are separated by boundary lines obtained by replacing $\tilde{v} = \pm 1$ into (24):

$$\tilde{b}(\tau+1) = \Gamma\tilde{b}(\tau) \mp \tfrac{1}{2}(1+\Gamma). \tag{27}$$

The region between these two boundaries corresponds to $\mathcal{R}_0$ and contains the $q = 0$ branch of (26). The upper and lower regions are, respectively, $\mathcal{R}_{-1}$ and $\mathcal{R}_1$ if $(1+\Gamma) > 0, \mathcal{R}_1$ and $\mathcal{R}_{-1}$ otherwise. A particular example of mapping and boundary lines is given in Fig. 3.

The elements of (26) are selected by setting the values of Γ, h_0 and h_1. Any real value, but Γ, is possible for h_q [see (9)]; however, we will consider only combinations of Γ, h_0 and h_1 leading to single valued mappings. The whole set of single valued mappings possible for the TDCC with $C = 0$ and $E = 0$ can be generated with the following graphic procedure (see Fig. 11). First draw the boundaries of the linear regions in the $(\tilde{b}(\tau), \tilde{b}(\tau+1))$ plane, which, for real R, can take any positive or negative slope. Then draw the $q = 0$ branch as a segment through the origin, with arbitrary slope and end points on the boundary lines. The $q = \pm 1$ branches compatible with the obtained configuration are the lines starting at the end points of the $q = 0$ branch which are completely contained in the $\mathcal{R}_{\pm 1}$ regions and lead to a single valued mapping Φ. An example of this procedure is shown in Fig. 11, where the lines leaving the end points of the $q = 0$ branch represent admissible branches of $\Phi_{h_0,h_1,\Gamma}$ in $\mathcal{R}_{\pm 1}$. The constraints of this procedure lead to the following relation that Γ, h_0 and $h_{\pm 1}$ must satisfy in order to define a single valued mapping

$$(h_0 < \Gamma \text{ and } h_{\pm 1} < \Gamma) \quad \text{or} \quad (h_0 > \Gamma \text{ and } h_{\pm 1} > \Gamma). \tag{28}$$

Denoting with $\{p_q\}$ the intersections of the three straight lines $\tilde{b}(\tau+1) = h_q\tilde{b}(\tau) + \Delta h_q$ with the line $\tilde{b}(\tau+1) = \tilde{b}(\tau)$, a point p_q is an actual (virtual) fixed point of $\Phi_{h_0,h_1,\Gamma}$ if it belongs (does not belong) to $\mathcal{R}_q$, moreover, it is a stable (unstable) fixed point if $|h_q| < 1$ ($|h_q| \geq 1$).

For $|\Gamma| < 1$, the possible configurations of $\{p_q\}$ are limited by the slopes of the boundary lines (27), and are such that only asimptotically stable, unstable or periodic behaviors are possible. Therefore, no chaotic behavior can be obtained from $\Phi_{h_0,h_1,\Gamma}$ for $|\Gamma| < 1$ (i.e., for $\zeta > 0$, or $R > 0$, since $Z \leq 0$ is unpractical) and $E = 0$.

In [1] a chaotic behavior is obtained for $|\Gamma| < 1$ by introducing the voltage generator E. When $E \neq 0$, (23) must be replaced with

$$\begin{aligned}\overline{\Lambda}_{Dq}[\tilde{v}(\tau) - E] + q(\overline{\Lambda}_{D0} - \overline{\Lambda}_{Dq})\\ = (1-\Gamma)\left[\tilde{b}(\tau) - \frac{E}{2}\right], \qquad q = -1, 0, 1.\end{aligned} \tag{29}$$

The resulting mapping $\Phi_{h_0,h_1,\Gamma,E}$, however, coincides with $\Phi_{h_0,h_1,\Gamma}$ after a suitable shift of the origin, i.e., by using the variables

$$\begin{aligned}\hat{v}(\tau) &= \tilde{v}(\tau) - E\\ \hat{b}(\tau) &= \tilde{b}(\tau) - E/2\\ \hat{b}(\tau+1) &= \tilde{b}(\tau+1) + E/2.\end{aligned} \tag{30}$$

From a graphic point of view, this transformation means that $\Phi_{h_0,h_1,\Gamma,E}$, can be obtained by shifting $\Phi_{h_0,h_1,\Gamma}$ of, respectively, $+E/2$ and $-E/2$ along the $\tilde{b}(\tau)$ and $\tilde{b}(\tau+1)$ axes, which may also lead to skew tent mappings (e.g., see Fig. 3). In particular, the family of skew tent mappings defined by $-\infty \leq h_0 \leq -1, 0 \leq h_1 < \Gamma$ and any E such that $-[(1+\Gamma)/2(\Gamma - h_0)](1+h_0) < E < [(1+\Gamma)/2(\Gamma - h_0)](1-h_0)$ shows the period-adding phenomenon described in Fig. 11 of [1].

As an alternative possibility, chaotic dynamics can be obtained by assuming $|\Gamma| > 1$ (i.e., by introducing a negative R element). In this case, the slope of the boundary lines between the linear regions is larger than 1 or smaller than -1, and allows, among the possible mappings, also the whole family of tent functions (e.g., see Fig. 11).

APPENDIX II

In this Appendix we will prove the following theorem.

Theorem 1: In each region of linearity $R_q, q = -1, 0, +1$ the solution $\tilde{v}(\tau)$ of the set of differential-difference equations (10) and (11) (hereafter denoted as $\tilde{v}_q(\tau)$) can be expressed as

$$\tilde{v}_q(\tau) = \tilde{V}_{0q} + e^{-\Lambda_{Dq}\tau}[\tilde{v}_q(0) - \tilde{V}_{0q}] + \int_0^\tau e^{-\Lambda_{Dq}(\tau-\tau')}\Gamma \cdot \left[\frac{df(\tau')}{d\tau'} + \Lambda_{Nq} f(\tau')\right] d\tau' \qquad \tau \le 1 \tag{31}$$

$$\tilde{v}_q(\tau) = \tilde{V}_{0q} + \sum_k \operatorname{res}_{s=\Lambda_{kq}}[W_q(s)\exp(s\tau)] = \tilde{V}_{0q} + \sum_k p_{kq}(\tau)\exp(\Lambda_{kq}\tau) \qquad \tau > 1 \tag{32}$$

where

- $\tilde{V}_{0q}$ represents the equilibrium point, possibly virtual, of region q, obtained by setting $d\tilde{v}_q/d\tau = 0$ in (10):

$$\tilde{V}_{0q} = 2\frac{\Gamma - 1}{\Gamma + 1}\left[\frac{\Delta h_q}{1 - h_q} - 0.5E\frac{1 + h_q}{1 - h_q}\right] \tag{33}$$

- $f(\eta) = \tilde{v}(\eta - 1) - \tilde{V}_{0q}, (0 < \eta < 1)$ denotes the initial condition;
- the function $W_q(s)$ of the complex variable s is defined as

$$W_q(s) = h^{-1}(s)\left[(1 - \Gamma e^{-s})(\tilde{v}_q(0) - \tilde{V}_{0q}) + e^{-s}\Gamma(1 + \Lambda_{Nq})\int_{-1}^{0}\left[\frac{d\tilde{v}_q(\eta)}{d\eta} + \tilde{v}_q(\eta) - \tilde{V}_{0q}\right]e^{-s\eta}\, d\eta\right] \tag{34}$$

$$h(s) = s + \Lambda_{Dq} - \Gamma(s + \Lambda_{Nq})e^{-s}; \tag{35}$$

- "res" denotes the residue, Λ_{kq} are the eigenvalues in region $q, p_{kq}(\tau)$ is a polynomial in τ of degree $r - 1$ if Λ_{kq} is a root of multiplicity r (in particular, p_{kq} reduces to a constant if $r = 1$).

Proof: Combining (10) and (11), the following differential-difference equation is obtained:

$$\frac{dw_q(\tau)}{d\tau} + \Lambda_{Dq} w_q(\tau) = \Gamma\left[\frac{dw_q(\tau - 1)}{d\tau} + \Lambda_{Nq} w_q(\tau - 1)\right] \tag{36}$$

where $w_q(\tau) = \tilde{v}_q(\tau) - \tilde{V}_{0q}$.

For $0 < \tau < 1$, since $f(\tau) = w(\tau - 1)$, a direct integration of (36) yields (31).

As far as the case $\tau > 1$ is concerned, from (36) it is readily verified that $W_q(s)$, defined in (34), is the Laplace transform of $w_q(\tau)$. In order to perform the inverse Laplace transform of $W_q(s)$, it is worth noting that its singularities, i.e., the zeros of function $h(s)$ (35), are the roots of the characteristic equation (15), which have bounded real parts (e.g., see Section IV-A).

Thus, $w_q(\tau)$ is given by

$$w_q(\tau) = \int_{c-j\infty}^{c+j\infty} W_q(s)\exp(s\tau)\, ds \tag{37}$$

where c is a suitable real value, greater than the greatest real part of the zeros of $h(s)$.

In order to prove that (37) and (32) are equivalent, let us consider the following integral:

$$\frac{1}{2\pi j}\int_{c-j\infty}^{c+j\infty} h^{-1}(s)\exp(s\tau)\, ds \tag{38}$$

which can be written as

$$\sum_k \operatorname{res}_{s=\Lambda_{kq}}[h^{-1}(s)\exp(s\tau)] - \frac{1}{2\pi j}\lim_{N\to\infty}\int_{C_N} h^{-1}(s)\exp(s\tau)\, ds \tag{39}$$

where C_N is a semicircumference in the left-half plane of radius R_N and center $s = c$, containing all the zeros of $h(s)$, and such that $R_N \to \infty$ as $N \to \infty$. Moreover, from the relation $h^{-1}(s) = O(1/s)$ (i.e., there exists a positive constant γ such that $|h^{-1}(s)| \le \gamma/|s|$ for large values of $|s|$) it follows that

$$\left|\int_{C_N} h^{-1}(s)\exp(s\tau)\, ds\right| \le -\gamma\exp(c\tau)\frac{\pi}{R_N\tau}[\exp(-\tau R_N) - 1] \tag{40}$$

and therefore

$$\lim_{N\to\infty}\left|\int_{C_N} h^{-1}(s)\exp(s\tau)\, ds\right| = \lim_{R_{N\to\infty}}\left\{-\gamma\exp(c\tau)\frac{\pi}{R_N\tau}[\exp(-R_N\tau) - 1]\right\} = 0 \quad \forall\tau \ge 0. \tag{41}$$

Then, (37) can be written, according to (39)

$$\frac{1}{2\pi j}\int_{c-j\infty}^{c+j\infty} W_q(s)\exp(s\tau)\, ds = \sum_k \operatorname{res}_{s=\Lambda_{kq}}[W_q(s)\exp(s\tau)] - \frac{1}{2\pi j}\lim_{N\to\infty}\int_{C_N} W_q(s)\exp(s\tau)\, ds \tag{42}$$

where $W_q(s)$ is given by (34). By substituting (34) in (42), it is easily verified that:

$$\lim_{N\to\infty}\int_{C_N} W_q(s)\exp(s\tau)\, ds = 0 \qquad \tau > 1. \tag{43}$$

In fact, (41) yields

$$\lim_{N\to\infty}\int_{C_N} h^{-1}(s) w_q(0)\exp(s\tau)\, ds = 0 \quad \forall\tau \ge 0 \tag{44}$$

and therefore

$$\lim_{N\to\infty}\int_{C_N} h^{-1}(s)\Gamma w_q(0)\exp[s(\tau - 1)]\, ds = 0 \quad \forall\tau \ge 1. \tag{45}$$

Moreover the integral

$$\lim_{N\to\infty}\int_{C_N} h^{-1}(s)\Big[e^{-s}\Gamma(1+\Lambda_{Nq}) \cdot \int_{-1}^{0}\left[\frac{dw_q(\eta)}{d\eta}+w_q(\eta)\right]e^{-s\eta}\,d\eta\Big]\exp(s\tau)\,ds \quad (46)$$

satisfies the hypotheses of the Fubini-Lebesgue theorem (see [17, Proposition 28, p. 33]), and then can be written as

$$\int_{-1}^{0}\left[\lim_{N\to\infty}\int_{C_N} h^{-1}(s)\Gamma(1+\Lambda_{Nq})e^{s(\tau-1-\eta)}\,ds\right] \cdot\left[\frac{dw_q(\eta)}{d\eta}+w_q(\eta)\right]d\eta. \quad (47)$$

Due to (41), the above limit is zero for $\tau>1$. Finally by using (42), (44), (45), and the definition $w_q(\tau)=\tilde{v}_q(\tau)-\tilde{V}_{0q}$, (32) is readily derived.

APPENDIX III

In this appendix we summarize the proof of Proposition 1 of Section IV-A, which can be fully found in [14]. The proof is based on [11, Theorem 13.7], which gives a necessary condition and three sufficient conditions for the zeros of a characteristic functions $H(\Lambda)$, made of an exponential polynomial and having a principal term (see [11, ch. 13]), to have negative real part. Furthermore, the proof is more easily developed in the (Λ_{Dq},h_q) plane, and the results can be rephrased in the (θ,h_q) plane by means of (12) and (16). In the following, the necessary condition ([11, Theorem 13.7, formula 13.6.1]) will be denoted as condition (n), whereas the three sufficient conditions will be denoted as a), b), c) with the same notation of the cited theorem. The conditions refer to $H(\Lambda)$ evaluated for $\Lambda=jy$, being y a real variable.

We note that (15) has the principal term; for $\Lambda=jy$ the characteristic function assumes the form:

$$H(jy)=F(y)+jG(y) \quad (48)$$

$$F(y)=\Lambda_{Dq}\cos y - y\sin y - h_q\Lambda_{Dq} \quad (49)$$

$$G(y)=y(\cos y-\Gamma)+\Lambda_{Dq}\sin y. \quad (50)$$

Seven cases can be distinguished, according to the values of Λ_{Dq} and h_q. For each of them, the application of [11, Theorems 13.7 and 13.3] yields the results summarized in Table VI (for a complete proof, see [14]). These results support the picture shown in Fig. 12, where the (Λ_{Dq},h_q) plane is divided into two regions: in the dashed regions, all the roots of $H(\Lambda)$ have negative real part due to the fullfilment of the sufficient condition c), while in the complementary regions there exists at least one root with positive real part, because the necessary condition (n) is violated.

The two boundary curves γ_1 and γ_2 of Fig. 12 have the same parametric equation:

$$\Lambda_{Dq}=\frac{y(\cos y-\Gamma)}{\sin y}$$

$$h_q=\frac{1-\Gamma\cos y}{\cos y-\Gamma} \quad (51)$$

TABLE VI
COLLECTION OF THE SEVEN CASES USED IN THE PROOF OF PROPOSITION 1 IN THE (Λ_{Dq},h_q) PLANE. THE NUMBERED REGIONS ARE DEFINED IN FIG. 12

$\Lambda_{Dq}>0$	$h_q<-1$	$(\Lambda_{Dq},h_q)\in\{\text{region 1}\}$	(c) verified
		$(\Lambda_{Dq},h_q)\notin\{\text{region 1}\}$	(n) violated
	$\mid h_q\mid<1$		(c) verified
	$h_q>1$		(n) violated
$\Lambda_{Dq}<0$	$h_q<1$		(n) violated
	$h_q>1$	$(\Lambda_{Dq},h_q)\in\{\text{region 3}\}$	(c) verified
		$(\Lambda_{Dq},h_q)\notin\{\text{region 3}\}$	(n) violated

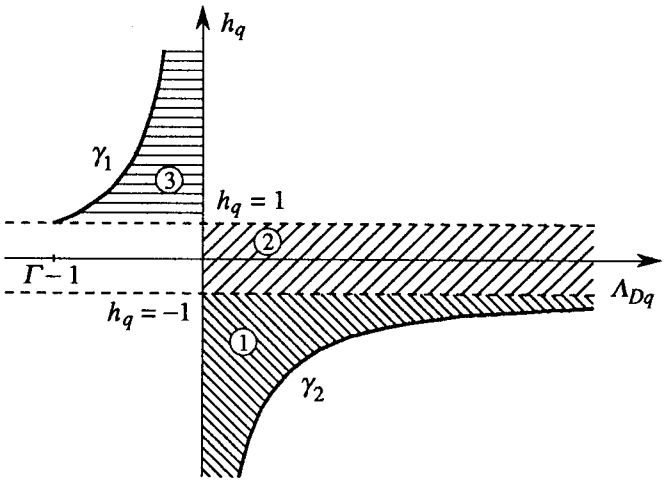

Fig. 12. Stability map in (Λ_{Dq},h_q) plane. In the dashed regions all the eigenvalues have negative real part, whereas outside there exists at least one eigenvalue with positive real part.

but are defined for different ranges of the parameter y:

$$\gamma_1: 0\le y<\arccos\Gamma \quad (52)$$

$$\gamma_2: \arccos\Gamma<y<\pi. \quad (53)$$

These expressions can be recasted in the form of (17)–(19) using (12) and (16).

ACKNOWLEDGMENT

The authors would like to thank L. Brino who drew the figures of this manuscript.

REFERENCES

[1] A. N. Sharkovsky, Yu. Maistrenko, P. Deregel, and L. O. Chua, "Dry turbulence from a time-delayed Chua's circuit," *J. Circuits Syst. Comput.*, vol. 3, pp. 645–668, June 1993.
[2] A. N. Sharkovsky, "Chaos from a time-delayed Chua's circuit," *Workshop on Chua's Circuit: Chaotic Phenom. Applicat.*, in *Int. Symp. Nonlinear Theory and Its Applicat.*, HI, USA, Dec 5–10, 1993, pp. 25–30.
[3] L. O. Chua, M. Komuro, and T. Matsumoto, "The double scroll family, parts I and II," *IEEE Trans. Circuits Syst.*, vol. 33, pp. 1073–1118, 1986.
[4] R. N. Madan, Ed., Special Issue on Chua's Circuit: A Paradigm for Chaos, *J. Circuits, Syst. Comput.*, vol. 3, Mar. 1993.
[5] ——, Special Issue on Chua's Circuit: A Paradigm for Chaos, *J. Circuits, Syst. Comput.*, vol. 3, June 1993.
[6] L. O. Chua, "Global unfolding of Chua's circuits", *IEICE Trans. Fundament. Electron. Commun. Comput. Sci.*, vol. E76-A, no. 5, pp. 704–734, May 1993.

[7] K. Murali and M. Lakshmanan, "Effect of sinusoidal excitation on the Chua's circuit," *IEEE Trans. Circuits Syst. I*, vol. 39, pp. 264–270, Apr. 1992.
[8] Y. L. Maistrenko, V. L. Maistrenko and L. O. Chua, "Cycles of chaotic intervals in a time-delayed Chua's circuit," *Int. J. Bifurc. Chaos*, vol. 3, pp. 1557–1572, Dec. 1993.
[9] A. N. Sharkovsky and E. Yu. Romanenko, "Ideal turbolence: Attractor of deterministic systems," *Int. J. Bifurc. Chaos*, vol. 1, pp. 31–36, Mar. 1992.
[10] M. Biey, F. Bonani, M. Gilli, and I. Maio, "On the effects of the capacitor in the time delayed Chua's circuit," in *Int. Symp. Nonlinear Theory and Its Applicat.*, HI, USA, Dec. 5–10, 1993, pp. 803–806.
[11] R. Bellmann and K. L. Cooke, *Differential-Difference Equations*. New York: Academic, 1963.
[12] E. A. Hosny and M. I. Sobhy, "Analysis of chaotic behavior in lumped-distibuted circuits applied to the time-delayed Chua's circuit," *IEEE Trans. Circuits Syst. I*, vol. 41, pp. 915–918, Dec. 1994.
[13] A. N. Sharkovsky, Yu. L. Maistrenko, and E. Yu. Romanenko, *Difference Equations and Their Applications*. Dordrecht, The Netherlands: Kluwer Academic, 1993.
[14] M. Biey, F. Bonani, M. Gilli, and I. Maio, "On the roots of the characteristic equation of a time delayed Chua's circuit," Internal Rep., Dipartimento di Elettronica, Politecnico di Torino, Italy, 1994.
[15] T. Matsumoto, L. O. Chua, and M. Komuro, "The double scroll," *IEEE Trans. Circuits Syst.*, vol. CAS-32, pp. 797–818, Aug. 1985.
[16] F. Zou and J. A.Nossek, "Bifurcation and chaos in cellular neural networks," *IEEE Trans. Circuits Syst. I*, vol. 40, pp. 166–173, Mar. 1993.
[17] L. Schwartz, *Methods Mathematiques Pour Les Sciences Physiques*. Paris, France: Hermann, 1965.

Mario Biey received the Dr. Eng. degree in electrical engineering from the Polytechnic of Turin, Turin, Italy, in 1967.

Initially, he was with the Istituto Elettrotecnico Nazionale Galileo Ferraris, Turin, as research engineer working on the application of optimization techniques to passive filter design. In 1971 he joined the Department of Electronics of the Polytechnic of Turin, where he is currently Professor of circuit theory. In 1984 and 1987 he was an Invited Professor with the Swiss Federal Institute of Technology, Lausanne. From 1986 to 1990, he was on the faculty of the University of Catania, Italy, as a Professor of basic circuit theory. He has been a consultant to several Italian industries in the areas of filter design and computer-aided-design and is a coauthor of the book *Tables for Active Filter Design* (Norwood, MA: Artech House, 1985). His main research areas have been passive and active filter design, approximation theory, and computer-aided-analysis of nonlinear circuits.

Fabrizio Bonani received the electronic engineering degree (cum laude) in 1992 from Politecnico di Torino, Italy.

Since then, he has been with the Electronics Department of the same institution, initially as a Ph.D. student and then, since 1995, as a Researcher. His research interests are mainly devoted to the physics-based simulation of semicondutor devices, with special emphasis on the noise analysis of microwave field-effect and bipolar transistors, and to the thermal analysis of power microwave circuits. He is also interested in the simulation of nonlinear dynamical systems. From October 1994 to June 1995 he has been a Consultant with the ULSI Technology Research Department of Bell Laboratories, Murray Hill, NJ, working on physics-based noise modeling of electron devices.

Dr. Bonani is a member of the IEEE Microwave Theory and Techniques and Electron Devices societies and the Associazione Elettrotecnica Italiana (AEI).

Marco Gilli received a degree in electronic engineering from the Polytechnic of Turin, Turin, Italy, in 1989.

He is currently a senior researcher with the Department of Electronics, Polytechnic of Turin, Turin, Italy. His research activity is mainly in the field of circuit theory, especially neural networks and nonlinear systems, and partially in the field of electromagnetic compatibility.

Ivan Maio received the Laurea degree and the Ph.D. degree in electronic engineering from the Polytechnic of Turin, Turin, Italy, in 1985 and 1989, respectively.

He is currently with the Department of Electronics at the Politecnico di Torino as a researcher. His research interests are in nonlinear and distributed circuits and in electromagnetic compatibility.